Molecular Biology of the Cell
Vol. 13, 2810–2825, August 2002

Structure of the Golgi and Distribution of Reporter Molecules at 20°C Reveals the Complexity of the Exit Compartments

Mark S. Ladinsky,* Christine C. Wu,†‡ Shane McIntosh,† J. Richard McIntosh* and Kathryn E. Howell*§

*Boulder Laboratory for 3-D Fine Structure, Department of Molecular, Cellular, and Developmental Biology, University of Colorado, Boulder, Colorado 80309; and †Department of Cellular and Structural Biology, University of Colorado Medical School, University of Colorado, Denver, Colorado 80262

Submitted December 26, 2001; Revised April 24, 2002; Accepted May 1, 2002
Monitoring Editor: Juan Bonifacino

Incubating cells at 20°C blocks transport out of the Golgi complex and amplifies the exit compartments. We have used the 20°C block, followed by EM tomography and serial section reconstruction, to study the structure of Golgi exit sites in NRK cells. The dominant feature of Golgi structure in temperature-blocked cells is the presence of large bulging domains on the three trans-most cisternae. These domains extend laterally from the stack and are continuous with "cisternal" domains that maintain normal thickness and alignment with the other stacked Golgi cisternae. The bulging domains do not resemble the perpendicularly extending tubules associated with the trans-cisternae of control cells. Such tubules are completely absent in temperature-blocked cells. The three cisternae with bulging domains can be identified as trans by their association with specialized ER and the presence of clathrin-coated buds on the trans-most cisterna only. Immunogold labeling and immunoblots show a significant degradation of a medial- and a trans-Golgi marker with no evidence for their redistribution within the Golgi or to other organelles. These data suggest that exit from the Golgi occurs directly from three trans-cisternae and that specialized ER plays a significant role in trans-Golgi function.

INTRODUCTION

The Golgi complex is the central organelle of the secretory pathway in eukaryotic cells (Palade, 1975; Farquhar and Palade, 1998). It is a ribbon-like structure composed of stacks of flattened, adherent cisternae (Rambourg and Clermont, 1997). Movement of molecules to, through, and from the Golgi complex occurs by several mechanisms, including vesicular and tubular transport as well as maturation and progression of the cisternae themselves (Bonfanti *et al.*, 1998; Hirschberg *et al.*, 1998; Martinez-Menarguez *et al.*, 1999; Glick, 2000; Pelham and Rothman, 2000; Marsh *et al.*, 2001b). Light and electron microscopic studies have provided an understanding of the Golgi stack and Golgi-associated transport vehicles (Rambourg and Clermont, 1997; Orci *et al.*, 1998; Lippincott-Schwartz *et al.*, 2000). However, the structures involved in exit processes at the trans side of the Golgi stack are less well defined. The most widely accepted view is that a tubular network continuous with the trans-most cisterna, a trans-Golgi network (TGN), is the compartment in which molecules are sorted and subsequently exit from the Golgi complex (Griffiths and Simon, 1986; Mellman and Simons, 1992).

A more complete structural understanding of Golgi exit sites is necessary for developing functionally accurate models for sorting and transport of molecules in the secretory pathway. In previous studies, we have used rapid-freezing and freeze-substitution technologies, in conjunction with high-voltage electron microscope (HVEM) tomography, to reconstruct regions of the Golgi ribbon in three dimensions (3-D) at ~7-nm resolution (Ladinsky *et al.*, 1994, 1999; Marsh *et al.*, 2001a). This approach has proven valuable and even essential for the accurate interpretation of data obtained from lower resolution techniques. The results from our high-resolution work are particularly powerful when interpreted along side of real-time in vivo imaging studies, which provide information about the dynamics of movement of Golgi components but cannot resolve the structural complexity within the organelle (see review, Lippincott-Schwartz *et al.*,

Article published online ahead of print. Mol. Biol. Cell 10.1091/mbc.01–12–0593. Article and publication date are at www.molbiolcell.org/cgi/doi/10.1091/mbc.01–12–0593.

§ Corresponding author. E-mail address: Kathryn. Howell@UCHSC.edu.

‡ Present address: Department of Cell Biology, Scripps Research Institute, La Jolla, CA 92037.

2000). NRK cells have been used for many of our studies of Golgi structure. In most cases each reconstructed Golgi region comprised seven cisternae, three of which were identified as trans by the following criteria. First, they present numerous tubules (often with budding profiles at their ends) that extend into the region trans of the Golgi stack, indicating that they are directly involved in exit processes. Second, a modified form of ER associates with all these cisternae. Finally, at least two types of trans-cisternae can be distinguished: one that produces exclusively clathrin-coated budding profiles and two that produce only non–clathrin-coated buds and tubules. The clathrin-associated cisterna has been the trans-most in all Golgi areas that we have studied.

The TGN has been defined as a tubular anastomosing compartment situated trans of the Golgi stack. It has been described as being continuous with either multiple trans-cisternae (Rambourg *et al.*, 1979) or with only the trans-most cisterna in the stack (Griffiths and Simons, 1986). In our studies of both chemically fixed (Ladinsky *et al.*, 1994) and rapidly frozen cells (Ladinsky *et al.*, 1999; Marsh *et al.*, 2001a), 3-D reconstructions have revealed tubules extending from multiple trans-cisternae but did not show this "traditional" TGN. However, the penultimate trans-cisterna in both cultured pancreatic beta cells (HIT-T15) and in freshly excised mouse islets of Langerhans appears as a tubular anastomosing compartment, consistent with the idea that extensive fenestration is a result of processes that consume the cisterna (Marsh *et al.*, 2001a, 2001b)

Our structural data suggest that transport out of the Golgi stack occurs from multiple trans-cisternae, not just from a single, trans-most cisterna. This is in contrast to commonly held views that a single, trans-most cisterna is the only exit site from the Golgi stack and that sorting of molecules destined to the plasma membrane from those destined to the endocytic/lysosomal pathway occurs in the trans-most cisterna or TGN (Bergmann *et al.*, 1981; Griffiths *et al.*, 1985; Mellman and Simons, 1992). This concept was developed largely from immunogold labeling experiments using VSV-G and other viral spike proteins as well as several endogenous transmembrane proteins. These studies showed that all cisternae, including the trans-most, appear to be labeled (see for example, Geuze *et al.*, 1984; Orci *et al.*, 1987). However, individual thin sections rarely reveal the full extent of the cisternae in a given Golgi stack, because of convolution of the membranes and the presence of openings in the cisternae, such as fenestrae and "holes" (Rambourg *et al.*, 1979; Rambourg and Clermont, 1990; Ladinsky *et al.*, 1999).

To further analyze the structure of the trans-Golgi, we have incubated NRK cells at 20°C, a condition reported to block exit from the Golgi and expand the TGN (Matlin and Simons, 1983; Matlin and Simons, 1984; Saraste *et al.*, 1986; Griffiths *et al.*, 1989). This article characterizes aspects of the Golgi structures that are affected by such a perturbation. Our results have implications for functional models of the exit sites from the Golgi stack.

MATERIALS AND METHODS

Cell Culture and 20°C Block Treatment

NRK cells were cultured at 37°C under 5% CO_2 in DMEM (Sigma-Aldrich, St. Louis, MO) supplemented with 10% fetal calf serum. For specimen preparation, cells were grown to ~75% confluency on Formvar-coated, carbon-stabilized, glow-discharged 100-mesh gold EM grids. For the 20°C block, the culture medium was further supplemented with 10 mM HEPES, and the samples incubated at 20°C for 4 h.

Rapid Freezing, Freeze-Substitution, and Sample Preparation

Cells were maintained at 20°C until just before freezing. Plunge-freezing and freeze-substitution were performed as previously described (Ladinsky *et al.*, 1999). Briefly, the EM grids with cells attached were rinsed for ~10 s in 20°C DMEM containing 5% Ficoll (70 kDa; Sigma-Aldrich), which served as an extracellular cryoprotectant. The grid was then hung with forceps in a plunge-freezing apparatus, blotted, plunged rapidly into a pool of liquid ethane chilled to −174°C with liquid nitrogen. Samples were freeze-substituted into acetone containing 1% glutaraldehyde and 0.1% tannic acid for 3 d at −90°C, and then slowly warmed to −50°C. The substitution solution was replaced with precooled acetone containing 2% OsO_4 and 0.01% uranyl acetate. These samples were allowed to warm from −50 to 4°C for >24 h, then rinsed three times in acetone, infiltrated into Epon-Araldite resin (Electron Microscopy Sciences, Port Washington, PA), and flat-embedded between two Teflon-coated glass microscope slides. Resin was polymerized at 60°C for >2 d.

Embedded samples were observed by phase-contrast light microscopy, and areas of apparently well-preserved cells were excised from the plastic "wafer" and remounted for cross-sectioning. Serial thin (40 nm) sections were cut on an UltraCut-UCT microtome (Leica, Inc., Deerfield, IL), transferred to formvar-coated copper-rhodium slot grids (EMS), stained with 2% aqueous uranyl acetate and Reynold's lead citrate, and observed on a Philips CM-10 transmission EM (Mahwah, NJ) to select suitable samples. Six sets of serial sections were recorded in their entirety for analyses complementary to the tomographic data (see Figure 6 and Table 1).

Blocks with regions of well-preserved Golgi were returned to the microtome. Ribbons of 6–12 serial 300-nm sections were cut, transferred to coated slot grids, and stained for 15 min with a saturated solution of uranyl acetate in 70% MeOH and then for 3 min with Reynold's lead citrate. Ten-nanometer colloidal gold particles were added to both sides of the grid (to facilitate aligning the series of tilted images). Then both sides of the grid were carbon-coated to enhance sample stability in the high-voltage electron beam.

HVEM and Dual-Axis Tomography

Procedures for HVEM image acquisition and dual-axis tomography were as described previously (Ladinsky *et al.*, 1999), with certain modifications. Grids were placed in a rotating, high-tilt stage and observed in a JEOL JEM-1000 (Peabody, MA) HVEM operating at 750 kV. A suitable Golgi region was imaged at ×12,000 with serial tilted views from +60° to −60° at 1.5° intervals using a Gatan 1k × 1k CCD camera. The grid was then rotated by 90°, and a similar tilt-series was taken. This procedure digitized an area corresponding to 1.42 μm^2 with a pixel size of 2.42 nm. Images were aligned, and a tomogram was computed from each tilt series. The single-axis tomograms were subsequently combined into one high-resolution tomogram for each thick section imaged (Mastronarde, 1997). The first tomographic dataset was based on a single section, whereas the second was based on two adjacent sections. In this case, two serial dual-axis tomograms were combined to yield a single dataset containing ~0.852 μm^3 of cellular volume.

The tomograms were modeled on Silicon Graphics Octane computers (Mountain View, CA.) using the IMOD software package (Kremer *et al.*, 1996). Each compartment in the Golgi region and all associated structures within the volume reconstructed were modeled individually in a distinct color. Details of manual and auto-

Table 1. Quantitation of Serial-Section Data

Data set[a]	Golgi cisternae detected[b]	Markers of polarity[c]	t-ER associating with these cisternae[d]	Bulges on cis/medial cisternae[e]	Trans-cisternae with bulges	Apparent bulge size[f]
1a	7	t-ER/C	T3	0	T1 = 1	+
					T3 = 2	+, ++
1b	>5[g]	t-ER/C	T1, T2, T3	0	T2 = 2	+, +
					T3 = 3	+, ++, ++
1c	7	t-ER	T2, T3	0	0	
2a	6	t-ER/C	T3	0	T3 = 1	+
					T1 = 2	+, +
2b	7	t-ER/C	T3	0	T2 = 2	+, ++
					T3 = 2	++, ++
					T1 = 1	++
3a	7	t-ER/C	T3	Possibly 1	T2 = 1	++
					T3 = 2	+, ++
					T1 = 1	++
3b	7	t-ER	T3	0	T2 = 1	++
					T3 = 1	+
4a	5	C		0	0	
4b	7	t-ER/C	T2, T3	0	T2 = 1	+
					T3 = 1	+
5a	7	t-ER/C	T2, T3	0	T2 = 1	++
					T3 = 1	++
5b	7	t-ER/C	T2, T3	0	T3 = 1	++
6	7	t-ER/C	T1, T2, T3	Possibly 1	T1 = 1	++
					T2 = 1	++

[a] Number indicates the set of serial sections used; letters distinguish different Golgi stacks visible within that set of sections.

[b] Cisternae in a Golgi stack were called "Golgi cisternae" unless they were continuous with membranes that bound ribosomes, whereupon they were called "ER."

[c] A cis-trans polarity was assigned to each stack based on the presence of clathrin (C), which associates only with the trans-most cisterna, or "trans-ER" (t-ER), which associated with 1–3 cisternae on the trans-side of the Golgi stack.

[d] As many as three cisternae on the trans-side of a stack associated with t-ER. Here we call the cis-most of these T1 and the more trans cisternae T2 and T3. In the nomenclature of Ladinsky *et al.* (1999) and Marsh *et al.* (2000), these are C5–C7, a terminology we cannot use here in all cases because of the uncertainty in the total number of cisternae, given serial sections instead of tomographic reconstruction.

[e] The term "bulge" was carefully defined above for tomographic reconstructions. With the comparatively less-complete data characteristic of serial section reconstruction, we have used a less formal, yet reliable method based simply on local shape. Regions defined as bulges are indicated with arrows in Figure 5.

[f] Bulge size is represented here with a qualitative indicator of size. Bulges that resembled the areas marked in Figure 5 are given one +. Larger bulges are assigned ++.

[g] The cisternae in this stack twisted, so not all could be clearly defined in this set of sections.

mated modeling and subsequent 3-D image display are described in Ladinsky *et al.* (1999).

Interpretation of Trans-Golgi Cisternae

Each trans-cisterna in the tomographic reconstructions was composed of distinct domains; these appeared either cisternal or "bulging." Once modeling of the Golgi regions was complete and the structures were viewed in 3-D, the domains were categorized by the following criteria. Cisternal domains were defined as those areas of a trans-compartment that had a luminal thickness equivalent to that of adjacent cisternae and that maintained their alignment with other cisternae in the Golgi stack. When viewed from their top or bottom, these domains were roughly constant in area and shape, and they varied little in their proximity to neighboring cisternae. "Bulging" domains were defined as regions of the compartment that extended laterally from the cisternal domain and showed no alignment with other Golgi structures. They appeared to open into volumes that were not constrained by cisternae or other organelles. These domains displayed significant increases in luminal thickness relative to the cisternal domains and showed nonuniform shapes that did not correspond to the neighboring cisternae. A line demarking these domains could easily be drawn through each trans-cisterna based on these criteria.

Immunoelectron Microscopy

NRK cells were prepared for immunoelectron microscopy as previously described (Ladinsky and Howell, 1992) with the following changes. Thin (90–100 nm) cryosections were cut with a cryodiamond knife (Diatome U.S., Port Washington, PA) at −110°C on an UltraCut-UCT microtome equipped with a FCS cryostage (Leica Inc.). Sections were picked up with a wire loop containing a drop of 2.1 M sucrose and 1% methylcellulose in PBS and transferred to formvar-coated, carbon-coated, glow-discharged 100-mesh copper-rhodium EM grids. Labeled cryosections were imaged on a Philips CM-10 TEM (80 kV) at ×21,000. Between 17 and 21 micrographs (final magnification: ×63,000) of each condition were quantitated by means of counting the gold particles per square micron of Golgi membrane.

Cell Fractionation and Immunoblots

NRK cells were grown at 37°C and shifted to 20°C for 4 h. The cells were harvested at ~75% confluency on ice by scraping in 0.2 ml immunoprecipitation (IP) buffer (50 mM HEPES, pH 7.3, 150 mM NaCl, 300 mM sucrose, and 2.5 μg/ml chymostatin, leupeptin, pepstatin A, and antipain). Cells were homogenized by 10 passes through an insulin syringe, and the nuclei were pelleted by centrifugation at 1500 rpm in a microfuge for 5 min at 4°C. The postnuclear supernatant (PNS) was collected and solubilized in 1% Triton X-100/IP buffer for 90 min on ice. Aliquots equivalent to 10 μg protein were loaded onto a 10% SDS-PAGE gel and transferred onto Immobilon-P. Blots were immunostained with antibodies raised against the luminal (2F7) and cytoplasmic domains of TGN38, MG-160, GMx33′, and the cation independent mannose-6-phosphate receptor and detected with enhanced chemilluminescence (ECL). Signal intensities were quantified by densitometry.

RESULTS

3-D Reconstructions of Regions from the Golgi Ribbon in 20°C Blocked NRK Cells

NRK cells were blocked at 20°C for 4 h, fixed by plunge-freezing followed by freeze-substitution, then analyzed by HVEM tomography at ~7-nm resolution, and modeled using the IMOD software. Regions of the Golgi ribbon from two different cells were reconstructed and modeled. A single slice (~2.4 nm thick) from each tomogram is shown in Figure 1, A and B. These tomograms represent regions from Golgi ribbons that differ significantly from one another. In Figure 1A the Golgi appears roughly circular; it lies close to the plasma membrane, adjacent to a large lysosome that contains a cholesterol crystal. Three regions of stacked and aligned cisternae, together with associated ER, are punctuated by large openings that contain numerous budding profiles and vesicles. The trans-faces of the stacks (defined by the adherent specialized ER and/or the presence of clathrin-coated buds) point outward from the center of the circle, whereas the *cis*-faces point inward. The second tomogram (Figure 1B) contains a large, crescent-shaped Golgi stack with two large openings and two smaller "substacks," the continuities of which are not apparent in this volume. The Golgi stacks in both tomograms are composed of seven cisternae, which is the same number found in the control NRK cells that we have analyzed (Ladinsky *et al.*, 1999). Others also have found that the number of cisternae in a stack does not change during 15 and 20°C perturbations (Volchuk *et al.*, 2000). However, when viewing individual thin sections or tomographic slices, not every cisterna is apparent. This is due to variations in the Golgi stack, particularly the presence or absence of openings in cisternae or variations between the stacked and unstacked domains along the length of the Golgi ribbon. In contrast, by viewing a Golgi region contained within the volume of a complete tomographic reconstruction, the number of cisternae in a stack could be determined with confidence. Although a serial-section reconstruction may represent the same (or more) volume as an equivalent tomogram, each section is thicker and the amount of structural change from one section to the next is much greater. Therefore, in the serial-section data sets included in this study the three last cisternae on the trans side of the Golgi stacks present within the volume of each data set are referred to alternatively as C5, C6, and C7 (when all cisternae in the stack could be accounted for) or as T1, T2, and T3 (when the cisternae could be followed from the previous section, but not all cisternae in the stack were present in the section shown).

Models of Golgi structures and associated components in these tomographic reconstructions are shown in Figure 1, C and D. The model in C represents a volume of ~1.0 × 1.0 × 0.4 μm, whereas that in Figure 1D represents ~1.0 × 1.0 × 0.8 μm. Each object in the models is color-coded such that each color represents an equivalent cisterna in both reconstructions. The complete models display the complexity of the reconstructed Golgi regions, but details of fine structure and interconnectivities are obscured. Virtual "dissections" of the models, using tools available in the IMOD software, allow subsets of the models to be viewed without interference from neighboring objects (see Figures 3–5 for portrayal of such dissections illustrating structural changes in Golgi cisternae due to the 20°C temperature block).

Another slice from tomogram 1 is shown in Figure 2, overlaid with colored modeling contours. This image provides an overview of the structural changes to the Golgi ribbon that occur during a 20°C temperature block. The seven cisternae are well aligned in most areas. The lumens of the ER-Golgi intermediate compartment (ERGIC, yellow) and the *cis*-cisternae (C1, light green; C2, dark blue) are enlarged relative to their counterparts in untreated cells (see Ladinsky *et al.*, 1999). The medial cisternae (C3, rose; C4, bright green) are closely adherent and appear unchanged. The three trans-most cisternae (C5, pink; C6, bronze; C7, bright red) are characterized by aligned regions that are continuous with domains that bulge out parallel to the stack into areas that are not constrained by cisternae or other structures. This characteristic is illustrated most dramatically in this slice by C6 in the lower right side (arrow). Finally, the three trans-most cisternae, and especially the bulging domains, are associated with specialized ER (blue-gray) with ribosomes represented by small purple spheres.

The Dominant Feature of the 20°C Block Is Bulging Domains on the Three Trans-most Cisternae

The three trans-most cisternae in Golgi stacks from 20°C blocked cells are characterized by regions that are in register with the preceding medial- and *cis*-cisternae but are continuous with domains that bulge out parallel to the plane of the stack. A portion of C6, from tomogram 1 is detailed in Figure 3A. The bulging domain (right) is easily distinguished from the cisternal region that aligns with its neighbors. Both parts of this cisterna display non–clathrin budding profiles (gray stippling). Because the protein composition of the coat could not be inferred from its morphology, we use the term "non–clathrin budding profile" to refer to these structures. Portions of all three of the trans-most cisternae from tomogram 2 are shown in Figure 3B. All three display similar bulging domains protruding from aligned cisternal regions (arrows). Tubules that extend perpendicular to the trans-cisternae into areas trans of the Golgi stack, a predominant feature of trans-Golgi cisternae in control cells (Ladinsky *et al.*, 1999), are completely absent in 20°C blocked cells. Moreover, a TGN that is obviously distinguishable from the trans-cisternae is not present, just as in control cells. In the absence of tubules, it is likely that the bulging domains serve as reser-

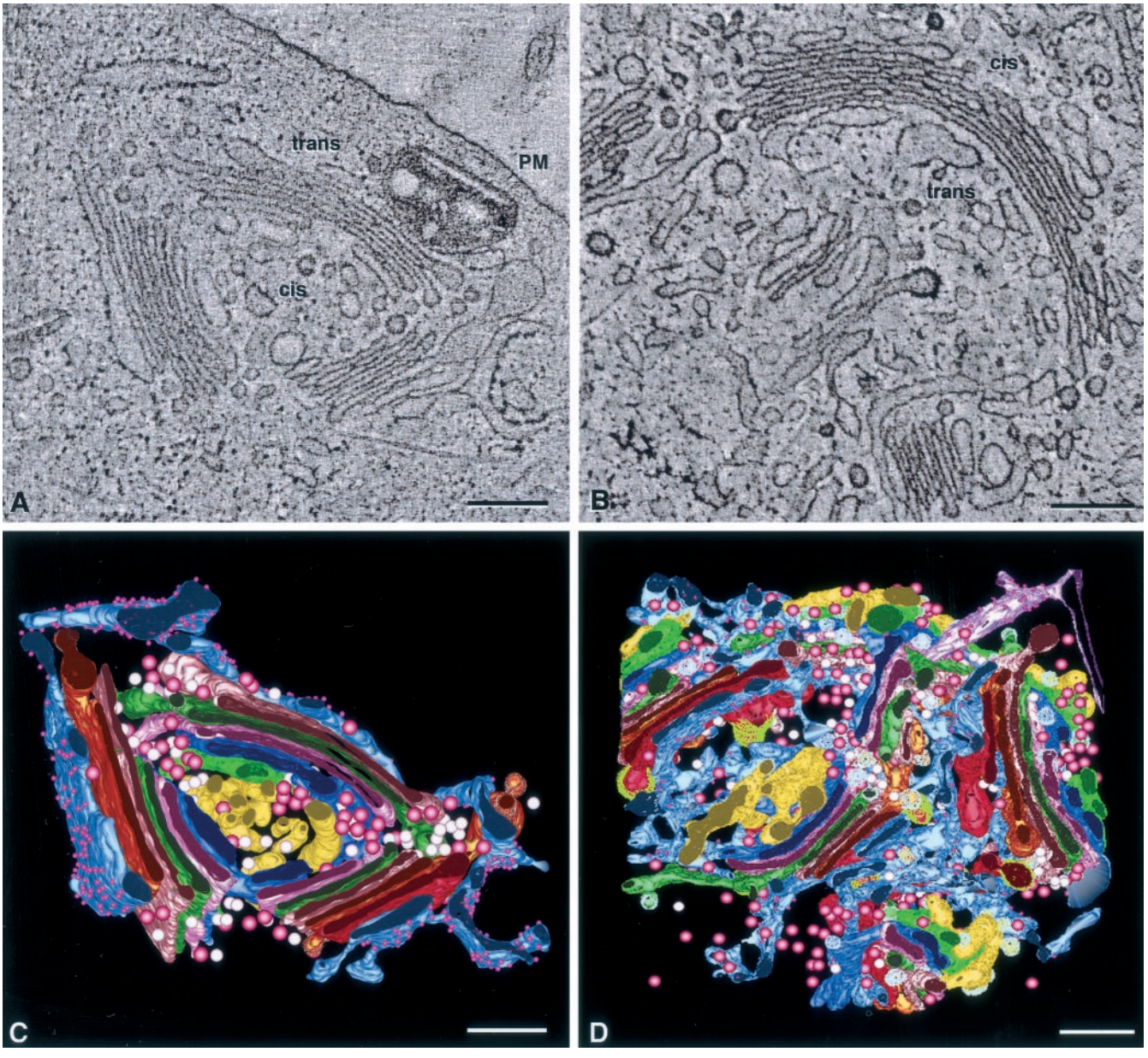

Figure 1. Overviews of tomographic reconstructions of regions of the Golgi ribbon in 20°C blocked NRK cells. (A) A single 2.4-nm tomographic slice from tomogram 1. Three stacked regions, punctuated by large openings, are aligned in a roughly circular configuration with the trans sides facing outward. There was no clathrin present in this region of the ribbon, but *cis*-trans orientation could be established by the presence of specialized ER that abuts the final cisterna in each stacked region. (B) Slice from tomogram 2. This complex Golgi is crescent-shaped and composed of three stacked regions. Large clathrin-coated buds indicate the trans-most cisternae in each region, and specialized ER confirms the orientation of the stack. Both ribbons are composed of seven cisternae, not all of which are visible in these views because of the thinness of the slices, fenestrations, and the convoluted nature of the Golgi ribbon. (C and D) Views of the completed model of each reconstruction. The complexity of the models makes interpretation difficult, necessitating virtual "dissection," shown in the following figures. Colors correspond to equivalent structures in both models: *cis*-side ERGIC/C1, yellow; C2, dark blue; C3, rose; C4, bright green; C5, pink; C6, bronze; C7, bright red; and specialized ER, blue-gray with purple spheres denoting ribosomes. Pink and white spheres denote free non–clathrin-coated and noncoated vesicles, respectively. Bars, 0.2 μm.

voirs for accumulated membrane and cargo molecules that cannot exit the Golgi due to the temperature block.

The cisternal and bulging domains of the trans-most cisternae could be clearly distinguished from one another. Each of the trans-most cisternae from tomogram 2 was displayed individually and rotated to an orientation most appropriate to show both domains (Figure 4). For each cisterna a line has been drawn to demarcate the two regions. Curiously, one or

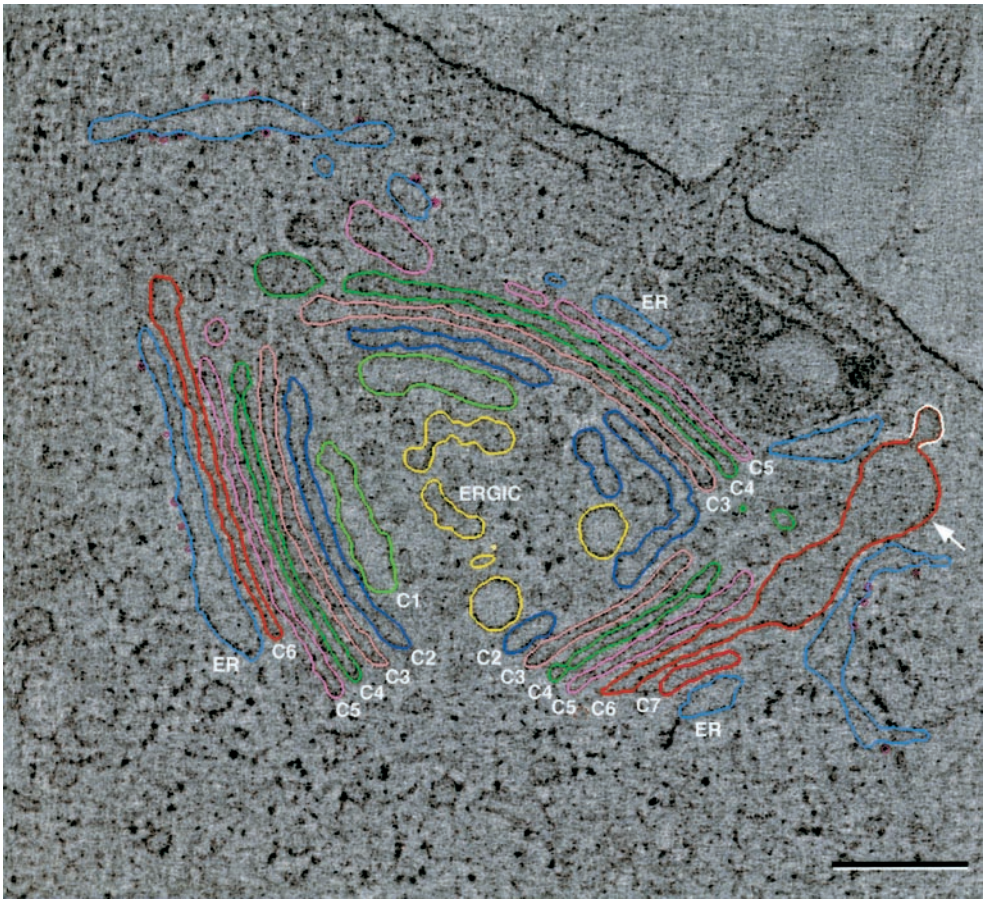

Figure 2. Slice from tomogram 1 with overlaid modeling contours. The IMOD software package, running on Silicon Graphics computers, was used to construct and model the tomographic data. Cisternae C1 and C2 are *cis*, C3 and C4 are medial, and C5, C6, and C7 are defined as trans. All cisternae are not present in each of the three stacked regions. C7 is absent from the left stacked region, and both C6 and C7 are absent in the upper right region, but all seven are present in the lower right region. Specialized ER is in contact with the last cisterna in each region. Two of the structural changes to the Golgi, characteristic of the 20°C block, can be noted in this image; the lumens of the ERGIC elements, C1 and C2, are uniformly enlarged relative to control cells. A large bulging domain, continuous with the aligned cisternal portion of C6 in the lower right region, is projecting laterally from the Golgi stack (arrow). All trans-cisternae in both reconstructions display similar bulging domains. Bar = 0.2 μm.

more fenestrae commonly lies on or near the demarcation line.

Clathrin Associates Exclusively with the Trans-most Cisterna

In 20°C blocked cells, as in control cells, clathrin buds are found only on the trans-most cisterna (C7, bright red in all model figures). This cisterna does not bear non–clathrin-coated buds, whereas C6 and C5 produce only buds with nonclathrin coats. Interestingly, the clathrin-coated buds in blocked cells are significantly larger than those in control samples. Figure 3C shows the C7 cisterna from a control cell bearing exclusively clathrin-coated buds (yellow stippling) that are approximately 100 nm in diameter. Figure 3D shows the equivalent cisterna from a temperature blocked cell, where the clathrin buds are ~300–500 nm in diameter. Although the budding profiles are larger, no differences in the structure or size of the clathrin spikes or in the pentagonal and hexagonal patterns of the triskelions on the surface of the buds could be discerned (Figure 3G). A parallel increase in the size of non–clathrin-coated buds is not observed in the *cis*- and medial-cisternae. Figure 3, E (control) and F (20°C block), show a C2 cisterna that bears nonclathrin buds of roughly equivalent size. All cisternae in 20°C blocked cells have fewer fenestrae than those in control cells.

Specialized ER Associates with Both Cisternal and Bulging Domains of the Three Trans-most Cisternae in 20°C Blocked Cells

In both control and 20°C blocked cells, specialized ER associates with trans-cisternae in a manner that resembles the association of Golgi cisternae with each other. This ER is continuous with the cell's RER network, but it is characterized by the presence of ribosomes only on faces that are nonadherent to Golgi cisternae. This specialized ER associates with all three of the trans-most cisternae, but not at the same place along the ribbon. In many cases the specialized ER associates with the portion of each trans-cisterna that is exposed or is trans-most in that region of the stack. This is illustrated in tomogram 1 (Figure 2), where in each of the three cisternal regions a different trans-cisterna is the last one in the stack: C5 in the upper right, C7 in the lower right, and C6 in the left region. In all three cases, the ER is adherent to the final, exposed, cisterna. In other regions, the ER associates with more than one trans-cisterna within a given volume. Figure 5A shows portions of the three trans-cisternae of tomogram 2, with ER associating with each of them in one place or another (arrows). In the 20°C blocked cells, the

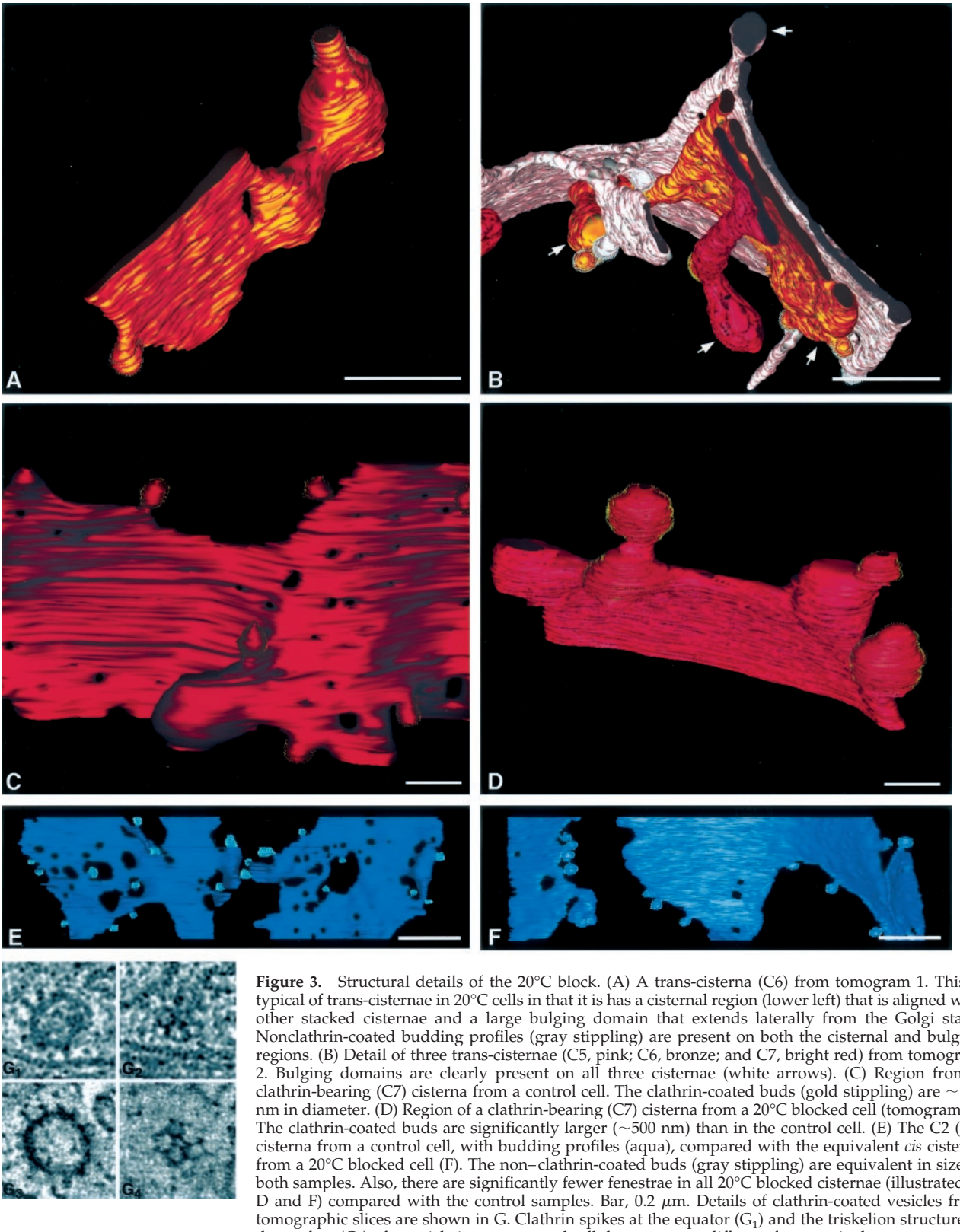

Figure 3. Structural details of the 20°C block. (A) A trans-cisterna (C6) from tomogram 1. This is typical of trans-cisternae in 20°C cells in that it is has a cisternal region (lower left) that is aligned with other stacked cisternae and a large bulging domain that extends laterally from the Golgi stack. Nonclathrin-coated budding profiles (gray stippling) are present on both the cisternal and bulging regions. (B) Detail of three trans-cisternae (C5, pink; C6, bronze; and C7, bright red) from tomogram 2. Bulging domains are clearly present on all three cisternae (white arrows). (C) Region from a clathrin-bearing (C7) cisterna from a control cell. The clathrin-coated buds (gold stippling) are ~100 nm in diameter. (D) Region of a clathrin-bearing (C7) cisterna from a 20°C blocked cell (tomogram 2). The clathrin-coated buds are significantly larger (~500 nm) than in the control cell. (E) The C2 (*cis*) cisterna from a control cell, with budding profiles (aqua), compared with the equivalent *cis* cisterna from a 20°C blocked cell (F). The non–clathrin-coated buds (gray stippling) are equivalent in size in both samples. Also, there are significantly fewer fenestrae in all 20°C blocked cisternae (illustrated in D and F) compared with the control samples. Bar, 0.2 μm. Details of clathrin-coated vesicles from tomographic slices are shown in G. Clathrin spikes at the equator (G_1) and the triskelion structure at the surface (G_2) of a vesicle in an untreated cell do not appear different from equivalent structures in a 20°C blocked cell (G_3 and G_4, respectively).

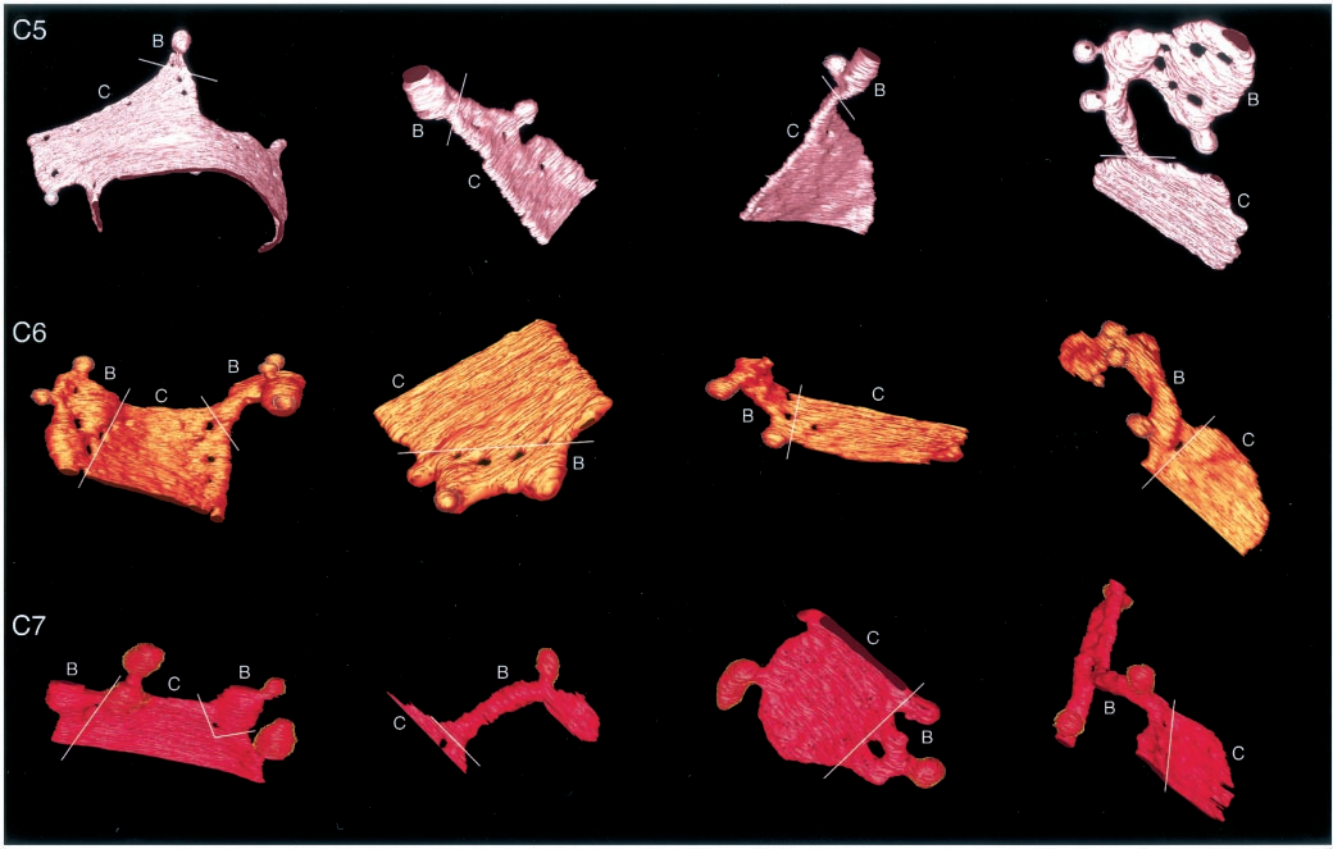

Figure 4. The trans-cisternae from tomogram 2. The various regions of C5, C6, and C7 cisternae displayed specific structural features, not present on preceding medial or *cis* cisternae, which allowed them to be categorized as trans. Each compartment was composed of "cisternal" (C) and "bulging" (B) domains. Cisternal domains remain aligned with and show luminal thickness equivalent to adjacent Golgi cisternae. Bulging domains show significant increase in luminal thickness, extend laterally from the cisternal domain, are nonuniform in shape, and show no alignment with other Golgi structures. They appear to extend into volumes that are not constrained by cisternae or other organelles. White lines demark the two domains on each compartment. One or more fenestrae often lie on or near the demarcation line.

specialized ER adheres very closely to, and often wraps around, the bulging domains of the trans-cisternae. Figure 5B shows this association with the large bulge on C6, tomogram 1.

Serial-Section Reconstructions

Regions from Golgi ribbons in 20°C blocked NRK cells were reconstructed, not only from tomograms but also from six sets of serial thin (40 nm) sections. Each set contained 3–6 distinct stacked Golgi regions. From these, 12 stacks were selected because their *cis*-trans orientations could be clearly defined by the presence of clathrin-coated buds, specialized trans-ER, or both. Ten serial sections are shown in Figure 6. Table 1 summarizes the serial-section data (the sections shown in Figure 6 represent dataset 6). In analyzing this data, first the orientation of the stack was established, the number of Golgi cisternae was counted, and the number and positions of trans-ER elements was noted. Then the number, position, and size of cisternal bulges was established. Seven cisternae were apparent in the stack in 9 of the 12 sets. In all but one data set, the ER was observed associating with one or more of the final three Golgi cisternae on the trans-side of the stack. Bulging domains were continuous with one or more of the final three cisternae on the trans side of the stack in all but one data set. The manner by which we defined "bulges" is detailed in MATERIALS AND METHODS. Possible bulging domains were detected on cisternae other than the final three in 2 of the 12 data sets.

The presence of bulges on many of the trans-cisternae in 20°C blocked cells motivated us to see whether there was a concomitant decrease in the size of the trans-cisternae themselves. To compare the cisternae in blocked vs. control cells, we selected five Golgi stacks from the samples described above that clearly showed seven cisternae and in which the length of each cisterna could be accurately measured. Five Golgi stacks from control cells were then identified to match the experimental sets as closely as possible. The length of each cisterna was then measured in every stack, excluding bulges if present, from the 20°C blocked cells. These measurements were examined individually (e.g., all C6s were compared between experiment and control, etc.) and in aggregate (all trans [C5–C7] or *cis*/medial [C1–C4] cisternae

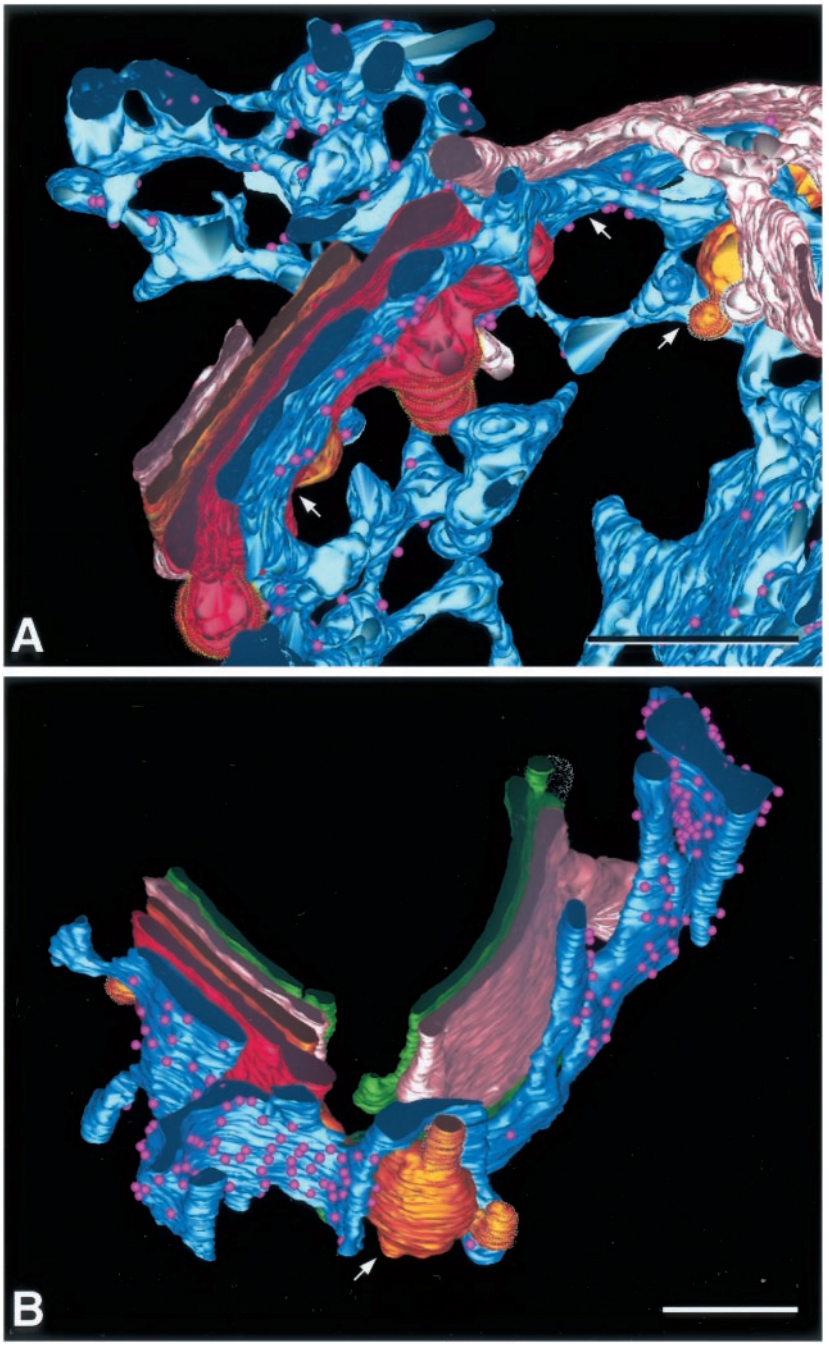

Figure 5. Association of specialized ER with multiple trans-cisternae . (A) Detail of the model of tomogram 2 showing C5 (pink), C6 (bronze), and C7 (bright red) trans-cisternae with ER associating with each (arrows). (B) Detail from tomogram 1 showing ER associating with C6 and C7. The ER is intimately wrapped around the large bulging domain (arrow) of the C6 cisterna. Bars, 0.2 μm.

similarly compared), but no statistically significant differences were detected. Given the variability of stack size, we also tried to normalize cisternal length by computing the average length of all cisternae in the section examined and then expressing the length of each cisterna as a ratio to the average. The ratios were then compared, both individually and pooled, to reflect all trans or *cis*/medial cisternae. Even with this approach, there were no detectable differences between experiment and control. The ratios of average trans-cisterna lengths to average total cisternal lengths were 0.98 ± 0.21 in controls vs. 0.94 ± 0.24 in 20°C blocked cells. For *cis*/medial cisternae the corresponding ratios were 1.01 ± 0.15 in controls vs. 1.05 ± 0.16 in 20°C blocked cells. We conclude that there is no evidence in our images for a consumption of cisternal membrane during the formation of trans-cisterna bulges.

In the serial section data sets, as with the tomographic data, the lumens of ERGIC elements and the first two cisternae on the *cis*-side of the stacks were uniformly enlarged relative to the other cisternae in the stack.

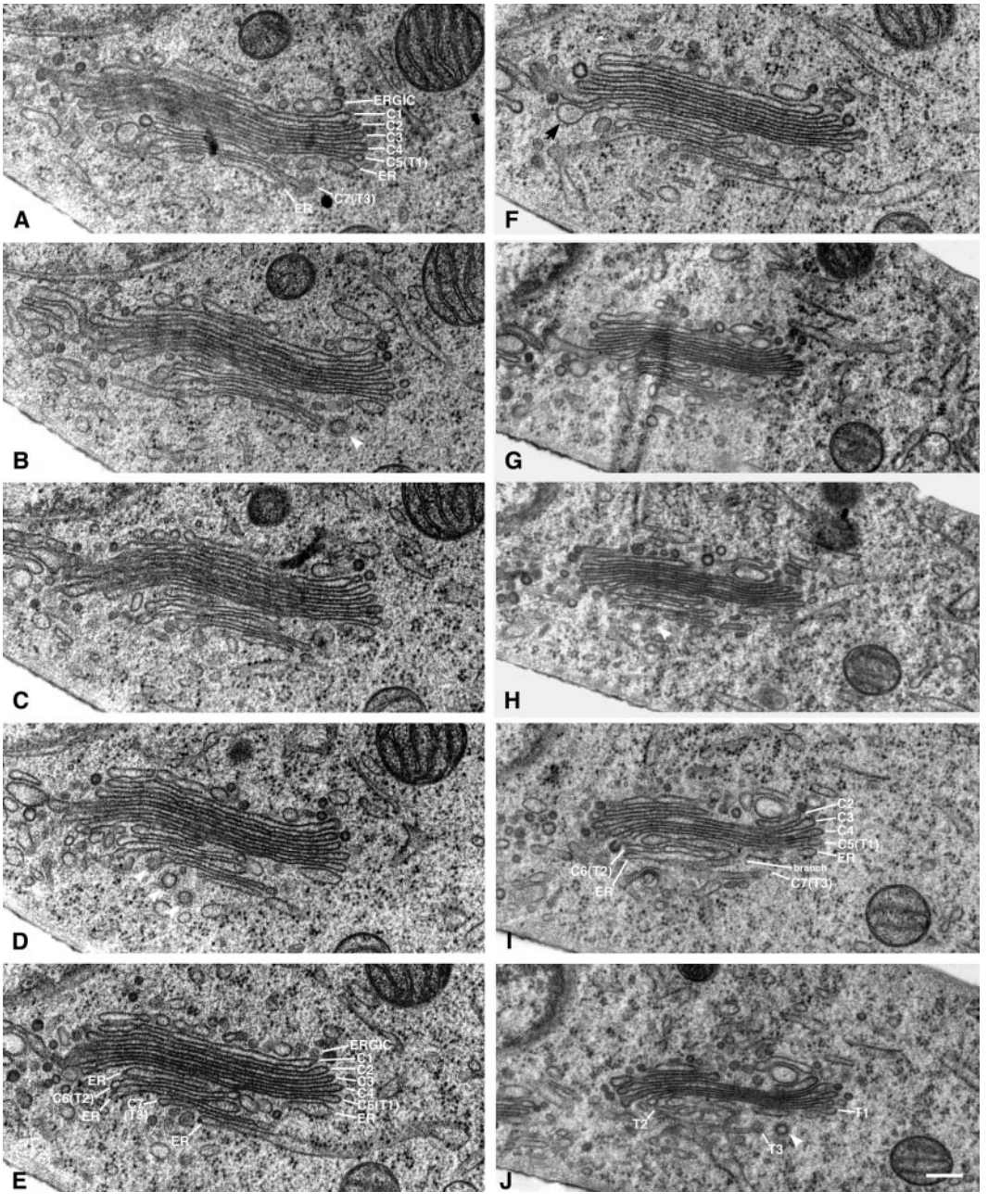

Figure 6. Ten serial sections (40 nm) through a Golgi stack from a 20°C blocked NRK cell. The stack consists of seven Golgi cisternae (ERGIC) and three branches of trans-ER associating with the three trans-most cisternae. The stack is oriented *cis*-to-*trans* from the top to the bottom of each panel. The cisternae are labeled in A, but the stack becomes ambiguous at its trans side, and C6 cannot be accurately distinguished from the intertwining ER. Thus, the C6 cisterna is not labeled in this panel. The final cisterna (C7) is clearly distinguished as it is associating with ER, is bearing a clathrin-coated bud, and there are no other Golgi cisternae trans of its position. Elements of the Golgi stack can be followed through the 10 panels. In E all cisternae and trans-ER elements can be distinguished from one another, and each is appropriately labeled. Although there are three ER elements associating with the three trans-most Golgi cisternae, the element located between C5 and C6 can easily be mistaken for a bona fide Golgi cisterna because it lacks ribosomes and does not directly connect to ribosome-bearing ER within this section. Following this element through to I, however, demonstrates that it is indeed ER because it connects to another part of the RER network by means of a branch that joins it with the ER element that lies between C6 and C7. Bulging domains are present on at least one of the three trans-most cisternae in this stack, most prominently in F, indicated by an arrow. Because there are seven cisternae in this stack, they could be labeled as C1–C7. However, this was not the case with all Golgi stacks analyzed by serial-section reconstruction; thus, the final three cisternae, C5–C7, were colabeled T1–T3, respectively. An apparent bulge present on the G4 cisterna in G likely represents a region of that cisterna that is bridging a gap between this stack and another that is outside of the field of view. Enlargements and distortions of cisternae in such bridging regions have been documented previously. Bar, 0.2 μm.

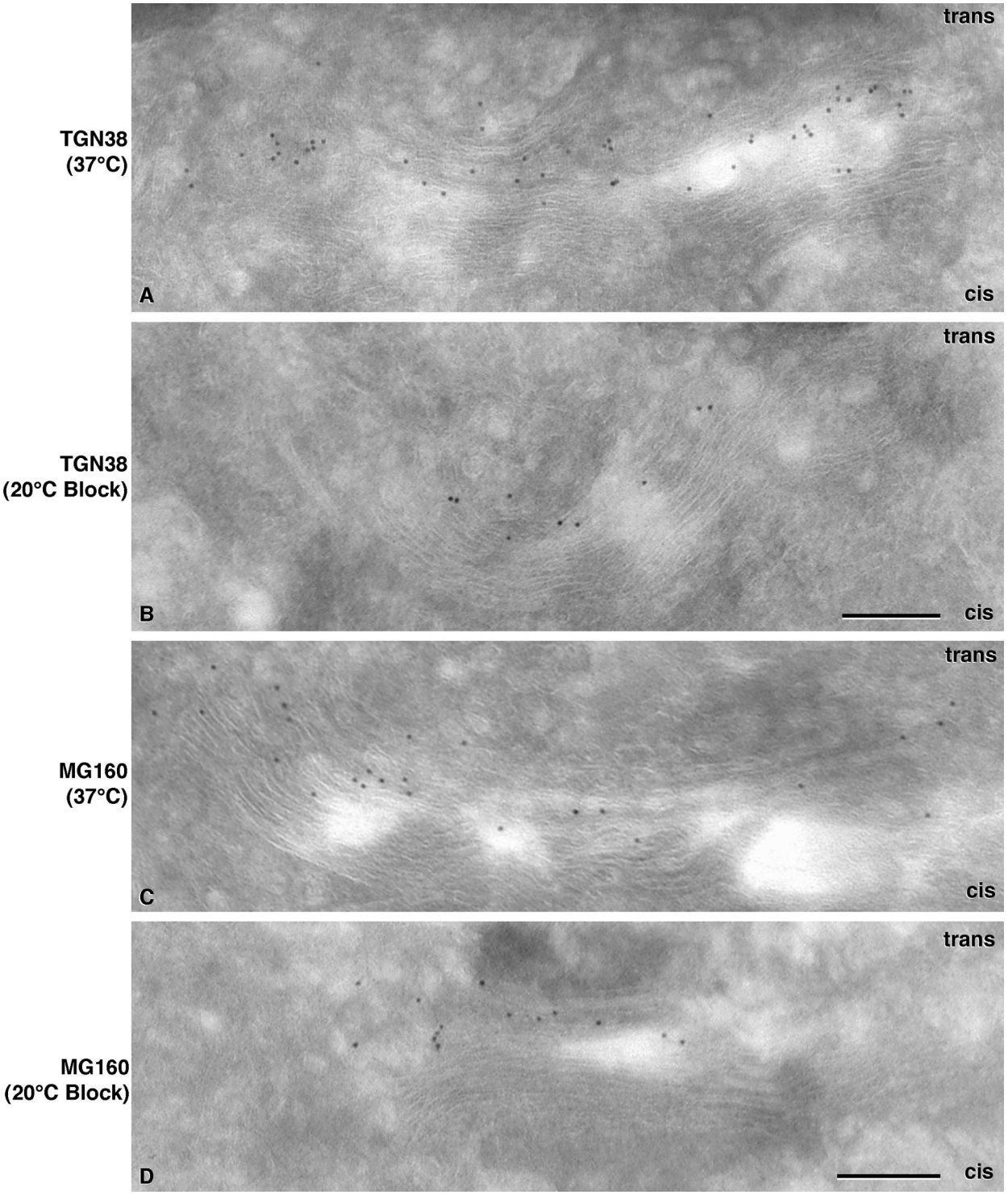

Figure 7. Localization of trans and medial Golgi markers in untreated and 20°C blocked cells. The trans-Golgi marker TGN38 is localized predominantly to the trans-cisternae in an untreated cell (A). The label is abundant and distributed evenly across the stack. TGN38 retains its localization to the final two to three cisternae in the Golgi stack of a 20°C blocked cell (B), but the amount of label detected is dramatically reduced from that of the control sample. MG160, a medial Golgi marker, localizes mainly to cisternae in the middle of the stack in untreated cells (C). Like TGN38, it retains this localization in the 20°C block (D), but the abundance of label is reduced. Bars, 0.2 μm.

Comparison of Medial- and Trans- Reporter Molecules in Control and 20°C Blocked Cells

Because the 20°C block resulted in obvious changes to the structure of the trans-cisternae, we investigated whether there were concomitant changes to or rearrangements of the localization of some medial and trans-Golgi markers. EM immunolocalization and immunoblot analyses of TGN38 and MG160 in control and 20°C cells were carried out to address these questions. TGN38 is a trans-Golgi marker that cycles to the plasma membrane and back, but it is predominantly localized to the trans-Golgi at any given time (Luzio *et al*., 1990; Ladinsky and Howell, 1992; Reaves *et al.*, 1993). MG160 is a marker of the medial Golgi that has homology to basic fibroblast growth factor receptor. It is sialylated but has not been shown to cycle to the plasma membrane (Gonatas *et al.*, 1989; Stieber *et al.*, 1995). In control cells, (Figure 7A), TGN38 is localized to the three trans-most cisternae. MG160 (Figure 7C) is mainly localized to the middle portions of the stacks with some label on trans-cisternae.

In 20°C blocked cells, both markers retained their positions within the stack relative to control cells (Figure 6, B and D). For each of the four conditions (labeling of cells cultured at 37 or 20°C, with antibodies to TGN38 or MG160) 17–21 micrographs were analyzed. Signal was assessed as the number of gold particles per square micrometer of cryosection in regions of the image that displayed Golgi stacks; areas without Golgi were used to assess background staining. Surprisingly, the density of each marker decreased during the 20°C block. TGN38 labeling decreased from 0.0446 ± 0.0216 gold particles/μm^2 in control cells (mean ± SD, corrected for an average background of ~0.0006 particles/μm^2) to 0.0144 ± 0.0079 particles/μm^2 in 20°C blocked cells, a 67% decrease. These metrics are based on 1432 and 401 gold particles scored on 21 and 20 micrographs, respectively. Background was measured on an area of 2.41×10^5 μm^2, and the average signal-to-noise ratio was 46. A two-tailed *t* test predicts that the probability that this difference could arise from two samplings of the same parent distribution is <0.001. The background-corrected density of MG-160 staining decreased from 0.0597 ± 0.0195 to 0.0453 ± 0.0170 particles/μm^2, a 24% decrease. On 18 and 17 sections, 1405 and 884 gold particles, respectively, were scored, background was measured on 2.17×10^5 μm^2, and the average signal-to-noise ratio was 48. The probability of the null hypothesis for these distributions is <0.02. Parallel changes in the distributions of either protein were not seen in any other compartment in the cell, for example, the plasma membrane or within the endosomal pathway (unpublished results).

An immunoblot analysis of postnuclear supernatant (PNS) from control and 20°C blocked cells is shown in Figure 8A. The corresponding quantification confirms the significant decrease of both TGN38 (60%) and MG160 (20%) that occurred during the temperature block. The use of a PNS for this analysis provides further evidence that neither marker was found in any abundance outside of their predominant Golgi locations. To ask whether all Golgi proteins are similarly degraded, we extended the immunoblot analysis to include two additional Golgi markers. Remarkably, the cationic independent mannose-6-phosphate receptor (CI-MPR), another transmembrane protein predominately localized to the trans-Golgi (Griffiths *et al*., 1988), and GmX33, a trans-matrix protein (Wu *et al.*, 2000) remained relatively constant, suggesting the degradation is selective. The steady state amount of both TGN38 and MG160 recovered within 2 h, demonstrating that the block is reversible.

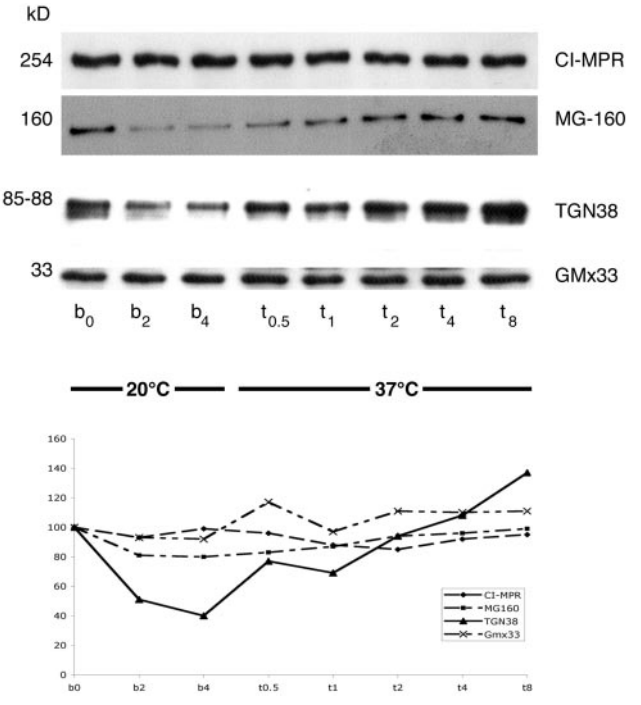

Figure 8. Immunoblot of Golgi markers in control and 20°C blocked NRK cells. Cells were blocked at 20°C for various times (*b* = 0, 2, and 4 h) then returned to 37°C for times (*t* = 0.5, 1, 2, 4, and 8 h). NRK PNS (10 μg) was prepared and loaded onto 10% polyacrylamide gels. The gels were subsequently transferred to Immobilon-P that was probed with specific antibodies and visualized with ECL. Bands were quantified by densitometry. These data are plotted below: CI-MPR (254 kDa and small diamonds), MG160 (160 kDa and small squares), the luminal domain of TGN38 (85–88 kDa and triangles with solid line), and Gmx33 (33 kDa and ×s). A duplicate blot was probed with antibodies against the cytoplasmic domain of TGN38 to determine if the protein was clipped rather than degraded, but no bands were detected (unpublished results).

DISCUSSION

During a 20°C temperature block, all of the cisternae in the Golgi ribbon undergo distinct structural changes, but the total number of cisternae in the stack remains unchanged from that of control cells. In the majority of our data sets, both control and experimental, there were seven cisternae in each Golgi stack. The Golgi cisternae in 20°C blocked cells differ from those in control cells by exhibiting fewer fenestrae, fewer budding profiles, and essentially no tubules extending from the cisternal margins or "holes." In addition to these general changes, there were specific changes to the *cis*- and trans-cisternae . There was a uniform enlargement in the luminal diameters of the *cis*-cisternae and of ERGIC elements near the *cis* face of the stack. Medial cisternae showed no distinct modifications. They maintained the same luminal diameter and adherence characteristics as

their counterparts in control cells. The changes to the trans-cisternae, however, were more dramatic. The last three cisternae at the trans-side acquired bulging domains that projected laterally from the stack. These bulges were continuous with "cisternal" domains that maintained a consistent luminal diameter and were aligned with the rest of the stack. There was often a cisternal opening located at the junction between the cisternal and bulging portions. The laterally projecting bulging domains were very different in structure from the exit tubules of trans-cisternae in control cells, which projected perpendicularly to the cisternae into the area trans of the Golgi stack. We initially anticipated that the number of exit tubules, which are always present in control cells, would be increased in 20°C blocked cells. Instead such tubules were not present at all in the volumes reconstructed for this study.

The bulging domains on the three trans-most cisternae constituted a significant increase in total luminal volume. The bulges most likely served as reservoirs for molecules that would normally have exited from those cisternae under physiological conditions. This interpretation was substantiated by the observation that in 20°C blocked cells, just as in control cells, non–clathrin-coated budding profiles were present on the C5 and C6 cisternae, whereas clathrin-coated buds were found exclusively on the trans-most cisterna (C7). The clathrin-coated buds on C7 were substantially enlarged compared with those in control cells while maintaining the normal structure of the clathrin triskelions. The nonclathrin buds remained approximately the same. These data suggest that budding and scission are affected differently by temperature and also that these steps differ in the clathrin and nonclathrin systems. These observations further support the hypothesis that proteins and lipids destined for different post-Golgi locations are sorted into multiple trans-cisternae, which themselves serve as the exit sites from the Golgi stack.

The 20°C block was originally characterized by following the transport kinetics of influenza virus hemagglutinin (HA) in MDCK cells (Matlin and Simons, 1983). This biochemical study showed that pulse-labeled HA was not detected on the cell-surface within a 2-h incubation at 20°C but that during this time the HA acquired complex oligosaccharides, implying that the protein accumulated in the trans-Golgi. When the temperature was returned to 37°C, the HA was transported to the cell surface within 25 min, demonstrating that the block was reversible. Parallel analysis with SDS-PAGE provided no indication of HA degradation during the temperature block.

Further characterization of Golgi dynamics during a 20°C block was carried out by EM-immunolabeling in two subsequent studies. These works focused on BHK cells infected with the temperature-sensitive form of VSV, tsO45, or with Semliki forest virus (SFV; Griffiths *et al.*, 1985, 1989). Both of these studies showed that at 20°C, VSV-G was present in all cisternae, but suggested that the trans-most cisterna was structurally altered by the accumulation of the G-protein and "extensive proliferation of the trans reticulum." In the first study, periodicity that corresponded to accumulated viral spike protein was observed in large, anastomosing tubular compartments. However, these compartments were distant from structures that labeled with clathrin antibodies, and there was no evidence of direct association between the two differentially labeled compartments. Therefore, by our criterion, the VSV-G containing structure cannot be interpreted as the trans-most Golgi cisterna. The second study presented a detailed morphometric analysis of immunolabeled cryosections in order to characterize which compartments in the secretory pathway expanded and which, if any, decreased in volume. The data indicated a significant expansion of the trans-reticular compartment and a parallel decrease in the surface area and volume of the Golgi stack. The trans-reticular compartment was called the TGN, which was described as containing both cisternal and tubular-reticular portions, the latter of which increased in size during the 20°C block (Griffiths *et al.*, 1989).

Our observation of bulges on the trans-cisternae of 20° blocked cells is consistent with the description of TGN enlargements by Griffiths *et al.* (1989), although the morphology of the change is different. Our morphometric studies showed an increase in membrane area in the bulging regions of the trans-Golgi but did not show a compensatory decrease in the membrane area of the cisternal domains.

Specialized ER Adheres to Multiple Trans-Cisternae

The presence of specialized ER adhering to all three trans-most cisternae both in control NRK (Ladinsky *et al.*, 1999) and pancreatic beta cells (Marsh *et al.*, 2001a, 2001b) as well as in the 20°C blocked NRK cells shown here suggests that this ER plays an essential a role in trans-Golgi function. This ER, which displays ribosomes only where is it not adherent to Golgi cisternae, was described in multiple cell types during the 1960s and 1970s as part of the structure called "GERL" (Golgi, ER, lysosomal; Novikoff, 1964; Novikoff *et al.*, 1971; Novikoff and Novikoff, 1977; Hand and Oliver, 1977). Later electron microscopy, using glucose-6-phosphatase reaction product to define the ER, showed clear association of ER with the trans-most cisterna in spermatids (Thorne-Tjomsland *et al.*, 1991). In our current study the unique way in which the ER is associated with, and in some cases actually wrapped around, the bulging domains of the three trans-most cisternae strengthens the case that this is a structure/function relationship that is crucial to trans-Golgi processes. We have proposed two possible functions for this specialized ER. It may be involved in modifying the lipid composition of trans-cisternal membranes for sorting into lipid rafts or "sphingolipid-cholesterol rich microdomains" (Simons and Ikonen, 1997; Brown and London, 2000). Additionally, the specialized ER may be involved in modifying the Golgi matrix to facilitate cisternal maturation (Wu *et al.*, 2000; Marsh *et al.*, 2001b). Perhaps the specialized ER, as it adheres to trans-cisternae, contributes enzymes that result in disassociation of the cisternae from the stack to facilitate the exit processes.

Degradation of Molecules during the 20°C Block

Our EM immunolabeling and immunoblot studies suggest that selective Golgi transmembrane proteins are degraded during the 20°C temperature block. This degradation is most pronounced with the trans-Golgi marker, TGN38, the amount of which was reduced by 60–70% during the 4-h block. The medial-Golgi marker MG160 showed less degradation (~20–25%), yet its decrease was still significant during this time. Immunogold labeling showed that TGN38 and MG160 remained relatively well localized to trans- and me-

dial-cisternae, respectively, and did not relocate to other cisternae or to other organelles during the 20°C block. This distribution indicates that the decrease of label in the Golgi was not due to movement of the markers to other compartments of the cell. The immunoblot data showed that these two marker proteins were not cleaved or overly sialylated, which are other factors that might account for the decrease in signal. Two other trans-markers were analyzed by immunoblot only: CI-MPR, a receptor characterized to leave the Golgi in clathrin-coated vesicles (Kornfeld and Mellman, 1989), and GMx33, a marker of the trans-Golgi matrix. Neither protein showed significant degradation.

During the temperature block the most profound structural changes and degradation of transmembrane markers occur in the trans-region. Griffiths and colleagues (1989) noted that during a 20°C block, the Golgi stack decreased in surface area and in volume much more than the TGN increased, and it was assumed that the excess membrane generated from this transformation accumulated in the ER. Because there was no apparent loss of their marker, VSV-G, degradation was not considered as an explanation for the membrane loss. Our data on the nonparallel loss of membrane proteins within the trans-Golgi region challenge the current concepts of protein turnover and will likely have an interesting explanation.

Why Do Our Data Differ from Previous Studies?

We have identified three possible factors that can explain why our observations of 20°C blocked Golgi structure are so different from those of Griffiths *et al.*, (1985, 1989). First, Griffiths' group used viral infections and used viral spike proteins as markers. This system may behave differently during a 20°C block than the endogenous molecules that normally transit the Golgi complex. The morphology in Griffith's studies shows that the accumulation of both VSV-G and SFV spike protein is so extensive that they form regular arrays; periodicity is apparent in many trans-Golgi regions in electron micrographs of both plastic and cryosections. In our studies a large number of endogenous proteins are blocked from exiting the Golgi, but no such regular arrays are apparent in either plastic or cryo-sections. These differing results may derive from a saturation of the secretory pathway by the viral spike protein, or they may be simply a result of massive expression of a single transmembrane protein. Hirschberg *et al.* (1998), however, argue that even with significant overexpression of VSV-G, the secretory transport pathway is never saturated. Nonetheless, the differences in morphology could be accounted for by the use of a single overexpressed exogenous protein in their studies. Our results demonstrate the effect of a 20°C block on endogenous constitutive secretion.

A second factor is the methods by which samples were observed and analyzed. Griffiths and colleagues used standard 2-D micrographs and stereological analysis, whereas we have used tomographic reconstruction, serial thin sections, and subsequent 3-D modeling. In individual (nonserial) thin sections, continuities of irregular, convoluted, and fenestrated compartments cannot easily be discerned, and it is often impossible to identify all of the cisternae in a Golgi stack or to clearly distinguish ER elements from Golgi cisternae. These points are illustrated in Figure 6. In contrast, serial thin sections, although lower in resolution than tomography, may be used to support and/or confirm results obtained from tomographic reconstruction. We thought it was important to demonstrate that the changes in the Golgi structure characterized by tomography could be confirmed in standard thin-section images. However, tomography is the preferable method because it permits 3-D visualization at ~6-nm resolution, allowing one to analyze structures and continuities with a high level of confidence and to study significant cellular volumes (McIntosh, 2001).

A third difference between these studies is the methods by which the cells were prepared for structural analysis. Griffiths and colleagues used chemical fixation techniques, whereas we used rapid freezing and freeze-substitution. Chemical fixation requires seconds or even minutes to stop all cellular processes, and different processes are immobilized at varying rates. This can result in artifactual alteration, especially of highly labile structures (Gilkey and Staehelin, 1986; Kellenberger *et al.*, 1992; McIntosh, 2001). Rapid freezing techniques uniformly immobilize the cells' contents within milliseconds, meaning that labile structures remain in place, and rapid processes, such as vesicle budding and tubule extension, are essentially halted in their native state (Dubochet, 1995).

It is likely that all three factors, viral infection, 2-D vs. 3-D analysis, and the difference in fixation methods, contributed to our distinctly different observations of Golgi structure during a 20°C temperature block.

CONCLUSION

To understand the mechanisms of sorting and exit from the Golgi complex it is essential to identify the specific structures in which these processes take place. The TGN was originally defined as the sorting and exit site from the Golgi, but its structure has not been clearly defined. Many think of it as the trans-most cisterna in the Golgi stack and an array of tubules that projects from it. Others interpret the TGN as an extension of the Golgi; a large anastomosing tubular network that "peels off" from multiple trans-cisternae (Rambourg and Clermont, 1990, 1997). Still others think of the TGN as an entirely separate organelle (Geuze and Morré, 1991; Reaves and Banting, 1992). Our 3-D structural data from rapidly frozen, freeze substituted samples of both control and 20°C blocked cells suggest that molecules are sorted in multiple trans-cisternae, each of which serves as an exit site from the Golgi stack. In this context, the TGN may be described as the final three cisternae in the Golgi ribbon and the exit tubules that extend from them.

ACKNOWLEDGMENTS

We thank Brad Marsh for critical reading of the manuscript and Mary Morphew, Eileen O'Toole, and David Mastronarde for helpful comments and suggestions through the course of the project. We also thank George Banting for the antibodies against the luminal domain of TGN38 (2F7) and Nicholas Gonatas for the antibodies against MG160. This project was funded by National Institutes of Health grant PO1-GM61306 to K.E.H. and J.R.M. and GM42629 to K.E.H.

REFERENCES

Bergmann, J.E., Tokuyasu, K.T., and Singer, S.J. (1981). Passage of an integral membrane protein, the vesicular stomatitis virus glycopro-

tein, through the Golgi apparatus en route to the plasma membrane. Proc. Natl. Acad. Sci. USA *78*, 1746–1750.

Bonfanti, L., *et al.* (1998). Procollogen traverses the Golgi stack without leaving the lumen of cisternae: evidence for cisternal maturation. Cell. *95*, 993–1003.

Brown, D.A., and London, E. (2000). Structure and function of sphingolipid- and cholesterol-rich membrane rafts. J. Biol. Chem. *275*, 17221–17224.

Dubochet, J. (1995). High-pressure freezing for cryoelectron microscopy. Trends Cell Biol. *5*, 366–368.

Farquhar, M.G., and Palade, G.E. (1998). The Golgi apparatus: 100 years of progress and controversy. Trends Cell Biol. *8*, 2–10.

Gilkey, J.C., and Staehelin, L.A. (1986). Advances in ultra-rapid freezing for the preservation of cellular ultrastructure. J. Elec. Microsc. Tech. *3*, 177–210.

Geuze, H.J., Slot, J.W., Strous, G.J., Hasilik, A., and Von Figura, K. (1984). Ultrastructural localization of the mannose 6-phosphate receptor in rat liver. J. Cell Biol. *98*, 2047–2054.

Geuze, H.J., and Morré, D.J. (1991). Trans-Golgi reticulum. J. Elec. Microsc. Techniques *17*, 24–34.

Glick, B.S. (2000). Organization of the Golgi apparatus. Curr. Opin. Cell Biol. *12*, 450–456.

Gonatas, J.O., Mezitis, S.G., Stieber, A., Fleischer, B., and Gonatas, N.K. (1989). MG-160, a novel sialoglycoprotein of the medial cisternae of the Golgi apparatus. J. Biol. Chem. *264*, 646–653.

Griffiths, G., Pfeiffer, S., Simons, K., and Matlin, K. (1985). Exit of newly synthesized membrane proteins from the trans cisterna of the Golgi complex to the plasma membrane. J. Cell Biol. *101*, 949–964.

Griffiths, G., and Simons, K. (1986). The trans Golgi network: sorting at the exit site of the Golgi complex. Science *34*, 438–443.

Griffiths, G., Hoflack, B., Simons, K., Mellman, I., and Kornfeld, S. (1988). The mannose 6-phosphate receptor and the biogenesis of lysosomes. Cell *52*, 329–341.

Griffiths, G., Fuller, S.D., Back, R., Hollinshead, M., Pfeiffer, S., and Simons, K. (1989). The dynamic nature of the Golgi complex. J. Cell Biol. *108*, 277–297

Hand, A.R., and Oliver, C. (1977). Relationship between the Golgi apparatus, GERL, and secretory granules in acinar cells of the rat exorbital lacrimal gland. J. Cell Biol. *74*, 399–413.

Hirschberg, K., Miller, C.M., Ellenberg, J., Presley, J.F., Siggia, E.D., Phair, R.B., and Lippincott-Schwartz, J. (1998). Kinetic analysis of secretory protein traffic and characterization of Golgi to plasma membrane transport in living cells. J. Cell Biol. *143*, 1485–1503.

Kellenberger, E., Johansen, R., Maeder, M., Bohrmann, B., Stauffer, E., and Williger, W. (1992). Artifacts and morphological changes during chemical fixation. J. Microsc. (Oxf.) *168*, 181–201.

Kornfeld, S., and Mellman, I. (1989). The biogenesis of lysosomes. Annu. Rev. Cell Biol. *5*, 483–525.

Kremer, J.R., Mastronarde, D.N., and McIntosh, J.R. (1996). Computer visualization of three-dimensional image data using IMOD. Struct. Biol. *116*, 71–76.

Ladinsky, M.S., and Howell, K.E. (1992). The TGN can be dissected structurally and functionally from the cisternae of the Golgi complex by brefeldin A. Eur. J. Cell Biol. *59*, 92–105.

Ladinsky, M.S., Kremer, J.R., Furcinitti, P.S., McIntosh, J.R., and Howell, K.E. (1994). HVEM tomography of the TGN: continuity of TGN with multiple trans cisternae and identification of a lace-like vesicle coat. J. Cell Biol. *127*, 29–38.

Ladinsky, M.S., Mastronarde, D.N., McIntosh, J.R., Howell, K.E., and Staehelin, L.A. (1999). Golgi structure in three dimensions: functional insights from the normal rat kidney cell. J. Cell Biol. *144*, 1135–1149.

Lippincott-Schwartz, J., Roberts, T.H., and Hirschberg, K. (2000). Secretory protein trafficking and organelle dynamics in living cells. Annu. Rev. Cell Dev. Biol. *16*, 557–589.

Luzio, P.J., Brake, B., Banting, G., Howell, K.E., Braghetta, P., and Stanley, K.K. (1990). Identification, sequencing and expression of an integral membrane protein of the trans-Golgi network (TGN38). Biochem. J. *270*, 97–102.

Marsh, B.J., Mastronarde, D.N., Buttle, K.F., Howell, K.E., and McIntosh, J.R. (2001a). Organellar relationships in the Golgi region of pancreatic beta cell line, HIT-T15, visualized by high resolution electron tomography. Proc. Natl. Acad. Sci. USA *98*, 2399–2406.

Marsh, B.J., Mastronarde, D.N., McIntosh, J.R., and Howell, K.E. (2001b). Structural evidence for multiple transport mechanisms through the Golgi in the pancreatic beta cell line, HIT-T15. Biochem. Soc. Trans. *29*, 461–467.

Martinez-Menarguez, J.A., Geuze, H.J., Slot, J.W., and Klumperman, J. (1999). Vesicular tubular clusters between the ER and Golgi mediate concentration of soluble secretory proteins by exclusion from COPI-coated vesicles. Cell *98*, 81–90.

Mastronarde, D.N. (1997). Dual-axis tomography: an approach with alignment methods that preserve resolution. J. Struct. Biol. *120*, 343–352.

Matlin, K.S., and Simons, K. (1983). Reduced temperature prevents transfer of a glycosylation. Cell *34*, 233–243.

Matlin, K.S., and Simons, K. (1984). Sorting of an apical plasma membrane glycoprotein occurs before it reaches the cell surface in cultured epithelial cells. J. Cell Biol. *99*, 2131–2139.

McIntosh, J.R. (2001). Electron microscopy of cells. a new beginning for a new century. J. Cell Biol. *153*, F25–F32.

Mellman, I., and Simons, K. (1992). The Golgi complex: in vitro veritas? Cell *68*, 829–840.

Novikoff, A.B. (1964). GERL, its form and function in neurons of rat spinal ganglia. Biol. Bull. *127*, 358.

Novikoff, P.M., Novikoff, A.B., Quintana, N., and Hauw, J.-J. (1971). Golgi apparatus, GERL and lysosomes of neurons in rat dorsal root ganglia studied by thick section and thin section cytochemistry. J. Cell Biol. *50*, 859–886.

Novikoff, A.B., and Novikoff, P.M. (1977). Cytochemical studies on the Golgi apparatus and GERL. Histochem. J. *9*, 525–551.

Orci, L., Ravazzola, M., Amherdt, M., Perrelet, A., Powell, S.K., Quinn, D.L., and Moore, H.P. (1987). The trans-most cisterna of the Golgi complex: a compartment for sorting of secretory and plasma membrane proteins. Cell *51*, 1039–1051.

Orci, L., Perrelet, A., and Rothman, J.E. (1998). Vesicles on strings: morphological evidence for progressive transport within the Golgi stack. Proc. Natl. Acad. Sci. USA *95*, 2279–2283.

Palade, G.E. (1975). Intracellular aspects of the process of protein secretion. Science *189*, 347–358.

Pelham, H.R., and Rothman, J.E. (2000). The debate about transport in the Golgi- two sides of the same coin? Cell *74*, 71–82.

Rambourg, A., Clermont, Y., and Hermo, L. (1979). Three-dimensional architecture of the Golgi apparatus in Sertoli cells of the rat. Am. J. Anat. *154*, 455–476.

Rambourg, A., and Clermont, Y. (1990). Three-dimensional electron microscopy: structure of the Golgi apparatus. Eur. J. Cell Biol. *51*, 189–200.

Rambourg, A., and Clermont, Y. (1997). Three-dimensional structure of the Golgi apparatus in mammalian cells. In: The Golgi

Apparatus, ed. E.G. Berger and J. Roth, Basel, Switzerland: Birkhäuser Verlag.

Reaves, B., and Banting, G. (1992). Perturbation of the morphology of the TGN following brefeldin A treatment: redistribution of a TGN-specific integral membrane protein, TGN38. J. Cell Biol. *116*, 85–94.

Reaves, B., Horn, M., and Banting, G. (1993). TGN38/41 recycles between the cell surface and the TGN: brefeldin A affects its rate of return to the TGN. Mol. Biol. Cell *4*, 93–105.

Saraste, J., Palade, G.E., and Farquhar, M.G. (1986). Temperature-sensitive steps in the transport of secretory proteins through the Golgi complex in exocrine pancreatic cells. Proc. Natl. Acad. Sci. USA *83*, 6425–6429.

Simons, K., and Ikonen, E. (1997). Functional rafts in cell membranes. Nature *387*, 569–572.

Stieber, A., Mourelatos, Z., Chen, Y.L., Le Douarin, N., and Gonatas, N.K. (1995). MG160, a membrane protein of the Golgi apparatus which is homologous to a fibroblast growth factor receptor and to a ligand for E-selectin, is found only in the Golgi apparatus and appears early in chicken embryo development. Exp. Cell Res. *219*, 562–570.

Thorne-Tjomsland, G., Clermont, Y., and Tang, X. (1991). Glucose-6-phosphatase activity of endoplasmic reticulum and Golgi apparatus in spermatocytes and spermatids of the rat: an electron microscopic cytochemical study. Biol. Cell *71*, 33–41.

Volchuk A., *et al.* (2000). Megavesicles implicated in the rapid transport of intracisternal aggregates across the Golgi stack. Cell *102*, 335–348.

Wu, C.C., Taylor, R.S., Ladinsky, M.S., Lane, D., and Howell, K.E. (2000). Gmx33, a novel family of trans-Golgi proteins identified by Proteomics. Traffic *1*, 963–975.